ARTICLE

The enhancement effect of oxygen vacancy on photocatalytic CO_2 reduction

Qiang Yang[a], Yunyi Wang[d], Qingwen Tian[a,c]*, Xiang Li[a], Aixiang Pan[a], Mengke Zhao[a], , Yawei Zhu[a], Ting Wu[a]*, Guigan Fang[a,b]* [c]

Experiment

Materials

Methanol (CH_3OH), bismuth nitrate ($Bi(NO_3)_3·5H_2O$), propanol ($CH_3CH_2CH_2OH$), ethylene glycol ($(CH_2OH)_2$), anhydrous ethanol (CH_3CH_2OH), 1-butanol ($C_4H_{10}O$), polyethylene glycol 200 (PEG200), potassium bromide (KBr) and polyethylene glycol 400 (PEG400) are ordered from Sinopharm Chemical Reagent Co., Ltd. Isobutanol ($C_4H_{10}O$) and tert-butanol ($C_4H_{10}O$) are obtained from Shanghai Lingfeng Chemical Reagent Co., Ltd. The lignin (Dealkaline) was produced from Tokyo Chemical Industry Co., Ltd.

Preparation of BiOBr with various contents of OVs

The photocatalysts were prepared by one-step solvothermal method according to our previous research[1], excepting that the type and ratio of alcohols have changed. Briefly, 0.476 g KBr and 0.0244 g lignin were dissolved in the mixed solutions composed of deionized water and anhydrous ethanol with different volume ratios, and the mixture above had 1.94 g of dissolved $Bi(NO_3)_3·5H_2O$. After agitating the mixture rapidly for 30 minutes, the homogeneously mixed solution was added to the Teflon-lined stainless autoclave, sealed, and allowed to react at 160°C for 12 hours. The catalysts were retrieved by centrifugation once they had cooled to room temperature. The obtained catalysts were then repeatedly cleaned with deionized water and anhydrous ethanol. These samples were then dried at 60°C for a full day. The anhydrous ethanol was substituted with other alcohols at the ratio of 40 to 10 based on the outcomes of the photocatalytic CO_2 reduction rection. All prepared catalysts were demonstrated in Table S1 and Table S2.

Characterization

X-ray diffraction (XRD, Ultima IV, Rigaku Co., Japan), Raman Spectrometer (RENISHAW INVIA, England) with an excitation line of 532 nm and Fourier transform infrared spectrometer (FT-IR, Thermo Scientific Nicolet iS5, USA) were carried out to characterize the phase structure and chemical composition of the sample. Transmission electron microscopy (TEM, FEI Talos F200X G2, USA) and scanning electron microscope (SEM, Zeiss Gemini 300) and energy dispersive spectroscopy (EDX) were utilized to observe the micromorphology, particle size and elements distribution of samples. N_2 sorption isotherms were used by a Micromeritics instrument (ASAP-2460, USA) to determine the samples' specific surface area and pore size distribution. The surface chemical states and chemical composition of catalysts were investigated using X-ray photoelectron spectroscopy (XPS, Thermo Scientific K-Alpha, USA). The oxygen vacancies (OVs) and ROS signals were probed by electron paramagnetic resonance spectrometer (EPR, Bruker A200, German). The photoluminescent (PL) spectra was conducted on a spectrofluorometer (F-4600, Hitachi, Japan). The UV–vis diffuse spectrophotometer (DRS, Shimadzu UV-3600i plus, Japan) was carried out to evaluate the energy band structures of the catalysts between conduction band (CB) and valence band (VB). The transient photocurrent (I-T), electrochemical impedance spectrum (EIS) and Mott-Schottky curve (MS) were measured0. on an electrochemical workstation (CHI 760e) coupled with a standard three-electrode cell.

Evaluation of Photocatalytic activity

40 mg of catalyst was dispersed into 20 ml of deionized water as reaction solution, and a 300 W xenon lamp equipped with a 420nm cut-off filter (Beijing Perfectlight Technology Co., Ltd). were used as the light source. A test of the optical power meter (CEL-NP2000-2A,

Beijing China Education Au-Light Technology CO., LTD) gives a light intensity of 86 W/cm^2. The Labsolar 6A (Beijing Perfectlight Technology Co., Ltd) equipped with a GC9790 II (Zhejiang Fuli Analytical Instruments Co., Ltd) was utilized to detect the products during the photocatalytic CO_2 reduction processes. A 200 mL sealed quartz round-bottom flask accompanying the Labsolar 6A instrument was utilized to hold the reaction solution, equipped with water circulation and a 5°C temperature. Before illumination, the entire system was subjected to a degassing process to remove impurity gases, and then CO_2 was bubbled into the system to achieve saturation for 10 minutes. The gas products were analyzed quantitatively by a GC9790 II equipped with a flame ionization detector (FID) at a 30-minute interval. After three hours of photocatalysis, the reaction was over.

Theoretical calculation

Applying the Perdew-Burke-Ernzerhof (PBE) formulation and the density functional theory (DFT) to the generalized gradient approximation (GGA), the energy band was computed. Projection augmented wave (PAW) potentials were carried out to analyze the ionic cores, and the valence electrons were considered with the aid of a plane wave basis set with a 450eV kinetic energy cutoff. Using the Gaussian smearing approach, Kohn-Sham orbitals with partial occupancies were allowed with a width of 0.05 eV. A convergence energy threshold of 10-5 eV was employed for the self-consistent computations, and the Brillouin zone integration was carried out with 6×6×6 Gamma k-point sampling to optimize the geometry and lattice size. The equilibrium geometries and lattice constants were optimized so that the maximum stress on each atom was less than 0.02 eV Å^{-1}. In Grimme's scheme, the DFT+D3 approach with empirical correction was used to characterize the weak interaction.

Table S1
Designations of prepared samples with deionized water and anhydrous ethanol.

V (anhydrous ethanol): V (deionized water)	0:50	10:40	20:30	30:20	40:10	50:0
Samples	BE0	BE10	BE20	BE30	BE40	BE50

Table S2
Designations of prepared samples with deionized water and other alcohols.

Reagents	Samples
Methanol	BM
Propanol	BP
1-Butanol	BB
Ethylene glycol	BEG
Polyethylene glycol 200	BPG200
Polyethylene glycol 400	BPG400
Isobutanol	BI
tert-Butanol	BT

Table S3
Different peaks binding energy of the O 1s XPS spectra, R (%) represents area ratio.

Sample	O1s (Bi-O)		O1s (O_V)		O1s (O_H)	
	Eb (eV)	R (%)	Eb (eV)	R (%)	Eb (eV)	R (%)
BE0	530.15	81.36	531.38	11.07	532.39	7.57
BE20	530.16	71.14	531.50	19.82	532.46	9.04
BE40	530.02	78.46	531.36	11.58	532.20	9.96
BE50	530.08	68.76	531.47	23.26	532.70	7.98
BEG	529.94	54.00	531.30	30.69	532.80	15.31

Table S4
Crystal size of different catalysts.

Samples	Crystallite size (nm)	Samples	Crystallite size (nm)
BE0	37.6	BP	20.6
BE10	24.6	BB	23.7
BE20	17.9	BEG	20.9
BE30	18.9	BPG200	6.8
BE40	25.8	BPG400	19.3
BE50	9.0	BI	23.8
BM	26.8	BT	18.3

Based on the XRD data fitting by *Jade* software, the crystallite size of all samples has been calculated through Scherer's equation. As shown in Table S3, the change trend of crystal size under the influence of solvent anhydrous ethanol is consistent with the oxygen vacancies intensity of EPR. When anhydrous ethanol is replaced by monohydric alcohol, the trend of crystal size still agrees with the EPR results. The crystal size of BEG with the best reductive efficiency is 20.9 nm, while BE50 with the second smallest crystal size has the worst CO_2 reductive performance. The photocatalytic effect is affected by various factors.

Table S5
Physicochemical structural parameters of different catalysts.

Catalysts	S_{BET} (m^2/g)	V_P (cm^3/g)	D_P (nm)
BE0	5.7738	0.036087	20.6863
BE40	24.8941	0.156298	22.2663
BE50	20.0681	0.114808	18.4276
BEG	40.8496	0.227418	20.9879

Table S6
The physicochemical characteristic of the samples.

Samples	Absorption edge (nm)	Energy gap (eV)
BE0	443.64	2.51
BE10	469.49	2.14
BE20	465.66	2.25
BE30	455.27	2.32
BE40	441.18	2.44
BE50	420.52	2.67
BM	447.20	2.45
BP	444.05	2.45
BB	438.44	2.55
BEG	519.52	2.39
BPG200	424.21	2.54
BPG400	425.58	2.62

Samples	Absorption edge (nm)	Energy gap (eV)
BI	442.82	2.51
BT	471.68	2.04

Table S7
The change of bond angle and bond length for the CO_2 molecules on BiOBr, BiOBr with OVs.

Catalyst	Ads-CO_2	
	C-O / Å	∠C-O-C
BiOBr	1.26	124.85
BiOBr with OVs	1.18	178.77

Table S8
The comparison of CO product rate over BEG in this study with other materials in the pure water.

Catalysts	CO yield (μmol $g^{-1}h^{-1}$)	Reference
This work	122.38	
MoO_{2-X} nanobelts	62.75	[2]
Bi_5O_7Cl	27.15	[3]
$BiOIO_3$	17.33	[4]
$Sr_2Bi_2Nb_2TiO_2$	17.11	[5]
$SrNb_2O_6$	16.60	[6]
ZnAl-LDH	7.60	[7]

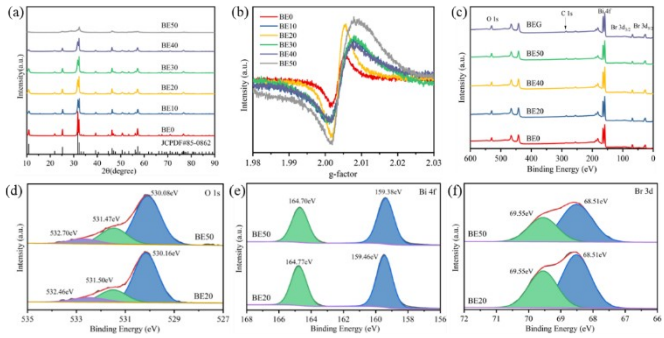

Fig. S1. XRD patterns(a), ESR spectra (b), the full-scan XPS spectra of BE0, BE20, BE40, BE50 and BEG (c), XPS spectra of BE20 band BE50 (d-f).

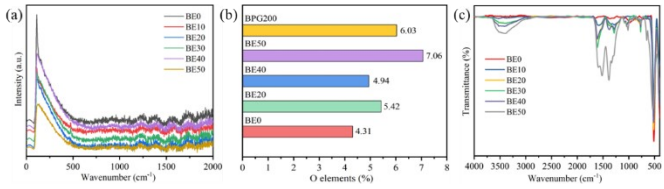

Fig. S2. Raman spectra (a), O element content by Elemental analyzer (CHNS/O) (b) and in-situ FTIRS spectra (c).

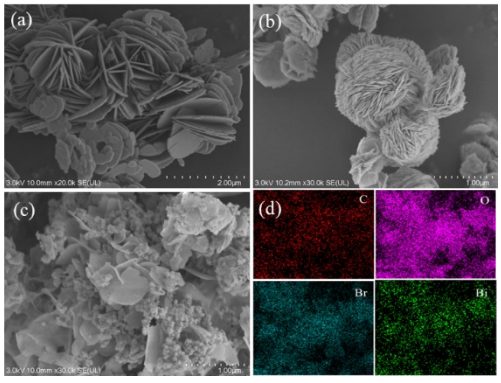

Fig. S3. SEM images of BE0 (a), BE20 (b), BE50 (c) and elemental mapping images of BEG (d).

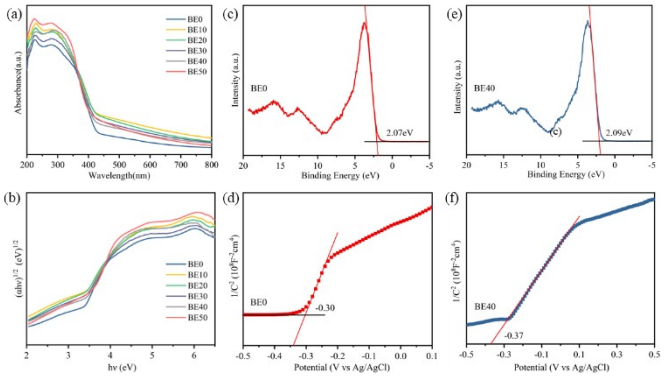

Fig. S4. DRS spectra (a), estimated band gaps (b), VB-XPS spectra (c, e) and Electrochemical Mott-Schottky plots (d, f) and of BE0 and BE40.

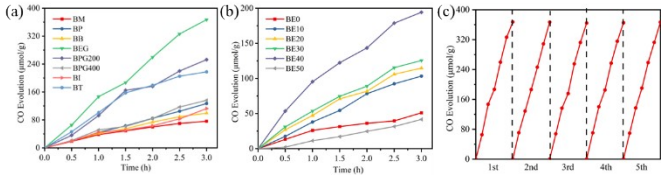

Fig. S5. Time-dependent CO yield (a-b), stability and recyclability of BEG for CO_2 reduction.

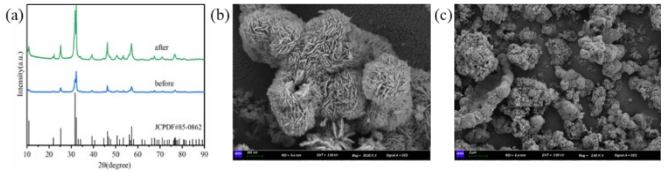

Fig. S6. XRD spectra (a), SEM images (b-c) after photocatalysis reactions.

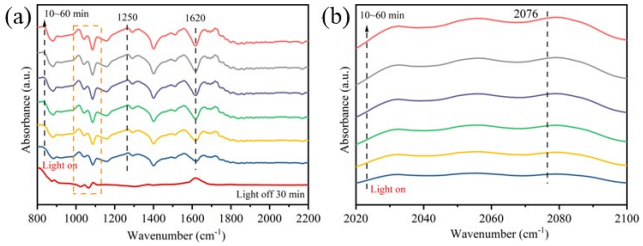

Fig. S7. In situ FTIR spectra of CO_2 and H_2O on the surface of BEG.

References

[1] Q. Yang, X. Li, Q. Tian, A. Pan, X. Liu, H. Yin, Y. Shi, G. Fang, J. Ind. Eng. Chem. 117 (2023) 117-129. https://doi.org/10.1016/j.jiec.2022.09.044.

[2] X. Liu, L. Yang, M. Huang, Q. Li, L. Zhao, Y. Sang, X. Zhang, Z. Zhao, H. Liu, W. Zhou, Appl. Catal. B, 319 (2022) 121887. https://doi.org/10.1016/j.apcatb.2022.121887.

[3] X. Shi, X.a. Dong, Y. He, P. Yan, F. Dong, Sci. Bull. 67 (2022) 1137-1144. https://doi.org/10.1016/j.scib.2022.01.013.

[4] F. Chen, Z. Ma, L. Ye, T. Ma, T. Zhang, Y. Zhang, H. Huang, Adv. Mater. 32 (2020) 1908350.

https://doi.org/10.1002/adma.201908350.
[5] H. Yu, J. Li, Y. Zhang, S. Yang, K. Han, F. Dong, T. Ma, H. Huang, Angew. Chem. Int. Ed. 58 (2019) 3880-3884. https://doi.org/10.1002/anie.201813967.
[6] S. Xie, Y. Wang, Q. Zhang, W. Deng, Y. Wang, Chem. Commun. 51 (2015) 3430-3433. https://doi.org/10.1039/C4CC10241J.
[7] Y. Zhao, G. Chen, T. Bian, C. Zhou, G.I.N. Waterhouse, L.-Z. Wu, C.-H. Tung, L.J. Smith, D. O'Hare, T. Zhang, Adv. Mater. 27 (2015) 7824-7831. https://doi.org/10.1002/adma.201503730.